RSC Advances

PAPER

View Article Online
View Journal | View Issue

Cite this: *RSC Adv.*, 2021, **11**, 7723

A straightforward and sensitive "ON–OFF" fluorescence immunoassay based on silicon-assisted surface enhanced fluorescence†

Ruohu Zhang, Zhanrui Jin, Zhengqiu Tian, Yingzhou Liu, Zhengqi Lu and Yiping Cui *

Received 14th October 2020
Accepted 8th February 2021

DOI: 10.1039/d0ra08759a

rsc.li/rsc-advances

A straightforward immunoassay based on silicon-assisted surface enhanced fluorescence (SEF) has been demonstrated using a silicon-based fluorescent immune substrate and silver-antibody nanoconjugate (SANC). The P-doped, (100) oriented silicon wafers are used for both fluorophore attachment and antigen immobilization. The silicon substrate offers a very low blank signal in the "OFF" state, due to its fluorescence quenching effect. In the detection process, the capture of the SANCs by the surface-immobilized antigen leads to an effectively enhanced fluorescence to produce an "ON" state. The analytical performance of the presented scheme has been investigated and a limit of detection of 31.4 pg mL^{-1} has been obtained. Besides the broadened application range compared with the conventional immunoassays, the presented scheme is straightforward, cost effective and sensitive, and is hence expected to find widespread applications in immunoassays as well as other fluorescence-based assays.

Introduction

Fluorescence spectroscopy is a powerful tool in medical and biological analysis.[1] Employing fluorescence to detect the biomarkers, or fluorescence immunoassay has become the technology of choice for the medical and clinical diagnostics.[2] For the early diagnosis of some diseases, a low concentration of biomarkers needs to be detected and quantified, so there is a continuing demand to improve the limit of detection (LOD) of a fluorescence immunoassay. Such improvement is generally closely related to an enhanced fluorescence signal intensity. The surface enhanced fluorescence (SEF) effect attracts a lot of attention and has been explored extensively to meet this need.[3–5]

The SEF effect, also known as the MEF (metal-enhanced fluorescence) effect, refers to the intensity enhancement of the fluorescence signals from the emitters in the proximity of metallic nanoparticles or nanostructures.[6–8] Besides the intensity enhancement, some other appreciable effects have also been observed, such as the decreased lifetime and the increased photostability.[9] Ever since the earliest theoretical studies in the 1980s,[10,11] much progress has been made in the understanding of the SEF effect. It is commonly accepted that several processes are involved, including an enhanced excitation field, an increased radiative decay rate of the emitter, as well as an increased coupling efficiency of the fluorescence emission to the far field through the nanoparticle scattering. The radiating plasmon model (RPM) has been raised by Lakowicz to address this latter issue,[12] and experimental evidences have also been observed recently.[13] Along with the better understanding in the mechanism, a lot of effort has also been made to push the SEF effect to real applications, including the SEF-based immunoassays.[14,15]

To date, various SEF-based immunoassay schemes have been successfully demonstrated, most of which consist of two separate components: the SEF substrate, and the immunoassay component same as that in the conventional fluorescence immunoassay scheme.[16–20] The SEF substrate has become the focus of the design. Different metallic nanostructures, such as silver island films,[16] self-assembled metallic nanoparticles[17,18] and metallic arrays[19] have been used as the SEF substrates. Despite the remarkable fluorescence enhancements obtained using these schemes, only a very few have demonstrated a significantly improved LOD.[17,19] The insufficient analytical performance in most such assay schemes is attributed to the inhomogeneity of the SEF substrates.[17] A kind of gold plasmonic substrate was recently developed by Dai *et al.* for SEF in the near-infrared region.[21–24] With improved homogeneity of the substrate, not only was the fluorescence greatly enhanced, but the LOD was also significantly improved. However, some other problems still exist. In the above assay architecture, a fluorescent labeled antibody is always used to detect the target antigen. Relatively complex chemistries are involved in the process of molecular labeling, which limits the application range and may also increase the overall cost of the immunoassay. In addition,

Advanced Photonics Center, Southeast University, Nanjing 210096, Jiangsu, China. E-mail: cyp@seu.edu.cn

† Electronic supplementary information (ESI) available. See DOI: 10.1039/d0ra08759a

the effect of labeling on the functionality of the antibody should also be evaluated.[25]

A different architecture of SEF-based immunoassay was raised by our group to address the above-mentioned issue. Instead of the conventionally used dye-labeled antibodies, the scheme used a fluorescent immune substrate and antibody functionalized silver nanoparticles to obtain the dose–responsive fluorescence signals, and was hence applicable to a wide range of antibodies.[26] The analytical performance was experimentally demonstrated. However, the LOD was moderate due to the strong inherent fluorescence of the substrate, which leads to a high blank signal. A higher blank signal generally leads to an increased standard deviation between multiple independent measurements, resulting in a higher LOD. Recently, metallic (Au or Ag) films has been introduced to replace the conventional substrate. Au or Ag films are known to strongly quench the fluorescence of the molecules in close proximity. Li *et al.* reported an Ag nanoantenna platform, in which Ag shell-isolated nanoparticles (SHINs) were used to enhance the fluorescence of the dye molecules previously assembled on an Ag film.[27] The pre-quenched fluorescence was subsequently enhanced by the Ag SHINs, and a significant enhancement of up to 10^5 was observed. Byrne *et al.* demonstrated a sensitive immunoassay using a similar methodology, where Au films were used for pre-quenching, and Au nanoparticle labeled antibodies were captured in the presence of the target antigens.[28] With the help of *in situ* grown Ag nanoparticles, a low LOD of 0.77 ng mL^{-1} was obtained. Despite the advantages brought by Ag or Au films, using these substrates in a practical immunoassay may be problematic. Special apparatuses such as evaporation systems are needed for film production, which adds complexity to the schemes. A straightforward, cost effective and sensitive immunoassay scheme is considered to have great potential.

The P-doped single crystalline silicon wafers have been reported to quench the fluorescence of the dye molecules near the silicon surface.[29] Silicon wafers are commercially available and cost effective due to the highly mature CMOS technology. Moreover, the use of silicon wafers renders the presented scheme the potential for integration with CMOS electronics. Although silicon-based SEF substrates have been reported recently, the quenching effect of the silicon substrate have rarely been explored for fluorescence enhancement.[30] Herein, a novel SEF-based immunoassay scheme is presented, wherein the silicon wafers are used instead of Au or Ag films for fluorescence quenching. The immunoassay scheme is shown in Fig. 1. The P-doped, (100) oriented silicon wafer has been used for both dye molecule attachment and antigen immobilization. This leads to the construction of a silicon-based fluorescence pre-quenched immune substrate, which offers a very low blank signal in the "OFF" state. The silver-antibody nanoconjugate (SANC) has been synthesized for specifically recognizing the surface-immobilized target antigens. In the process of detection, the capture of the SANCs by the surface-immobilized antigen leads to an effectively enhanced fluorescence to produce an "ON" state. The dose–responsive performance was also investigated. Benefiting from the low blank signal and the effective fluorescence enhancement, the LOD was determined to be 31.4 pg mL^{-1}, which is significantly lower than that obtained from the conventional substrate. The presented scheme is straightforward, cost effective and sensitive, and is hence expected to find widespread applications in immunoassays as well as other fluorescence-based assays.

Experimental

Materials

Polyethyleneimine (PEI), MW 15 000, 1-ethyl-3-(3-dimethylaminopropyl) carbodiimide (EDC) and *N*-hydroxysuccinimide (NHS) were purchased from Sigma-Aldrich. Rose bengal (RB) was purchased from Aladdin Reagent Co., Ltd. Silver nitrate ($AgNO_3$) and glutaraldehyde (GA) were purchased from Alfa Aesar. Trisodium citrate ($Na_3C_6H_5O_7 \cdot 2H_2O$) was purchased from Sinopharm Chemical Reagent Co., Ltd. Human immunoglobulin G (HIgG) and goat anti-human immunoglobulin (GaH-IgG) were purchased from Beijing Bioss Biotech Co., Ltd. Bovine serum albumin (BSA) were purchased from Nanjing KeyGEN Biotech. Co., Ltd. Polyoxyethylene (20) sorbitan monolaurate (Tween-20) and Tris (hydroxymethyl) aminomethane (TRIS) were purchased from Sinopharm Chemical Reagent Co., Ltd. The TBS buffer solution was prepared by dissolving NaCl (8.76 g) and TRIS (1.21 g) in water (500 mL). The TBS-T buffer solution was prepared by mixing Tween-20 (0.25 g) with TBS (500 mL). The BBS solution was prepared by dissolving sodium tetraborate in water to a concentration of 2 mM, reaching a pH of 9.0. P-doped, (100) oriented silicon wafers with a resistivity of 1–10 Ω cm were purchased from Suzhou Ruicai Semi-Conductor Co., Ltd. The water used in the experiments was ultrapure deionized water. All chemical reagents were used as received without further purification.

Preparation of Ag nanoparticles

Colloidal Ag nanoparticles were prepared according to the two-step method developed by Lu *et al.*[31] Briefly, an aqueous solution of $AgNO_3$ (1 mL, 0.3 M) was added to a solution of $Na_3C_6H_5O_7$ (4 mL, 0.46 M) at 70 °C and a pH of 11. The mixture was then vigorously sonicated until it appeared milky white, indicating the completion of the Ag seed formation. This Ag seed solution was subsequently syringed into a boiling solution of HNO_3 (295 mL, pH = 4.5) under stirring. The solution was kept heated for 1.5 h and then allowed to cool slowly to room temperature. The as-prepared Ag nanoparticles were purified several times by centrifugation and redispersion.

Preparation of the SANC

The SANC was prepared according to previously reported methods with some modifications.[26,32–34] The GaH IgG solution (70 μL, 1 mg mL^{-1} in BBS) was added to the purified Ag nanoparticles (1 mL) which was previously adjusted to a pH of 9.0 using K_2CO_3. The mixture was incubated at 37 °C for 1 h. Then a BSA solution (24 μL, 5% in BBS) was added and the mixture was incubated for another 0.5 h. Finally, the mixture was purified by centrifugation and redispersed in BBS (200 μL).

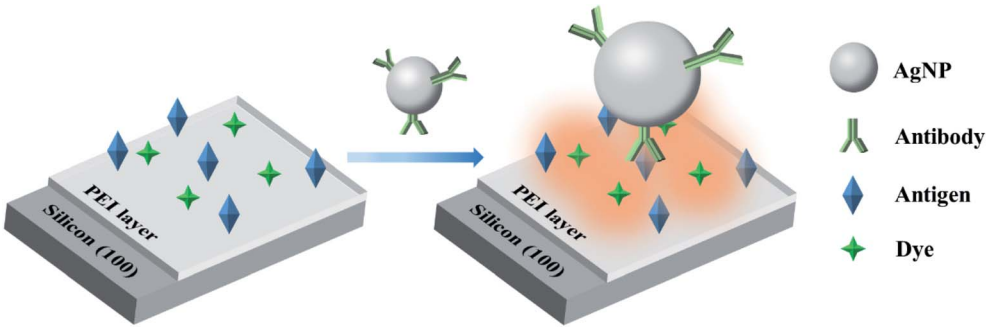

Fig. 1 Schematic of the "ON–OFF" fluorescence immunoassay based on the silicon-assisted surface enhanced fluorescence.

Preparation of the fluorescence pre-quenched immune substrate

The fluorescence pre-quenched immune substrates were prepared according to our previous report with some modifications.[26] The silicon wafers were cut into square pieces with each edge 2.0–3.0 cm. They were treated with a piranha solution (a 4 : 1 (v/v) mixture of H_2SO_4 (98%) and H_2O_2 (30%)) under sonication for 4 h to remove the impurities and to activate the surface. After rinsed with copious amounts of water and blow-dried with nitrogen, the cleaned silicon substrates were covered with sticky black tapes containing punched holes (9 mm in diameter) to form wells on the substrate surface. A fixed area for sample manipulating was hence defined on all the substrates in order for the quantitative analysis. PEI was subsequently assembled on the silicon substrates by pipetting the PEI solution (2 mg mL^{-1} in 0.5 M NaCl) into the wells at 100 μL per well followed by incubation for 15 min. After rinsing with water, RB was covalently immobilized on the PEI-attached silicon substrates *via* the EDC/NHS crosslinking protocol. Freshly prepared EDC (10 mM, 10 μL) and NHS (0.1 M, 2.5 μL) were mixed with an RB solution (100 μM, 1 mL) to activate the –COOH groups of the RB molecules. After incubated for 15 min at room temperature, the mixture was diluted with PBS to a concentration of 10 μM in terms of RB. The diluted solution was subsequently pipetted into the wells of the substrates. After 1 h's incubation in the dark at room temperature, the substrates were rinsed with water and blow-dried with nitrogen. A GA solution (5%) was then pipetted into the wells of the substrates and incubated for 3 h at room temperature. After thoroughly rinsed with water and dried under nitrogen, the fluorescence pre-quenched immune substrates were stored at 4 °C for future use.

Immunoassay procedures

HIgG of different concentrations were added to the wells of the fluorescence pre-quenched immune substrates. After incubated overnight at 4 °C in a humid chamber, the substrates were washed with TBS-T, TBS and water for three times, and then blow-dried with nitrogen carefully. Blocking was then performed with BSA (5% in PBS) for 3 h at room temperature. After washing with TBS-T, TBS and water for three times, the SANCs were added at 50 μL per well and incubated for 2 h in a humid chamber at room temperature. The substrates were then rinsed with water, dried with nitrogen and stored at 4 °C until measurement.

Determination of the fluorescence enhancement factor (EF) and quenching efficiency (QE)

The fluorescence EF is determined as the ratio of the fluorescence peak intensity of the RB-attached substrate with nanoparticles to that without nanoparticles. The fluorescence QE is defined as the percentage of the fluorescence intensity reduction due to quenching compared with the fluorescence intensity without quenching. The glass substrate was considered to be free of quenching effect and used as a control when attached with the same surface density of RB as the silicon substrate. To ensure that the surface densities of RB are the same on both substrates, an indirect method was employed as follows. After the incubation with RB the substrates were washed with water and the washing solution was collected. The absorption spectrum of the washing solution was measured and compared with that of the incubation solution which had been diluted to the same volume. According to the difference in the peak absorbance of the two solutions, the molar extinction coefficient of RB, as well as the surface area of the well on the substrate, the surface density of the attached RB can be determined. By choosing the proper deposition conditions, the surface density of RB on the glass substrate was adjusted to be the same as that on the silicon substrate.

Characterization

The extinction spectra were measured with a Shimadzu UV-3600 PC spectrophotometer. Quartz cuvettes of 10 mm path length were used for measurement and the pure water was used as a control. The fluorescence spectra were measured with an Edinburgh FLS 920 spectrometer equipped with a 450 W xenon lamp. The excitation wavelength was set to 520 nm. The front-face geometry was used for the measurement where both the excitation and the detection were performed form the front side of the substrate. The power of the excitation at the sample surface and the illuminated sample area were measured to be 0.17 mW and 7 mm^2, respectively. The integration time was set to 0.5 s. To eliminate the interference of the background noise,

another substrate similarly prepared to the sample substrate but without RB attachment was used as a background control.

TEM images characterizing the size and shape of the Ag nanoparticles and the SANCs were taken with a transmission electron microscope (FEI Tecnai G^2 F20, Holland). SEM images characterizing the surface morphology of the SANC-attached substrates were taken with a scanning electron microscope (Hitachi S-3000N, Japan). Thickness measurements were performed using a spectroscopic ellipsometer (Horiba Uvisel).

Results and discussion

Characterization of the SANC

Ag nanoparticles have been shown to exhibit highly efficient SEF effect and were hence chosen for the enhanced fluorescence immunoassay. Despite the various preparation methods, few of them yield Ag nanoparticles with satisfactory uniformity of size and shape, which imposes limitations on the controllable SEF applications.[35] The Ag nanoparticles used in our work were prepared according to a recent report, where the nucleation stage and the growth stage of Ag nanoparticles have been skillfully separated.[31] The TEM image of the as-prepared Ag nanoparticles is shown in Fig. 2a, where spherical Ag nanoparticles with a similar size can be clearly observed. The size distribution of the Ag nanoparticles is shown in Fig. 2b, which was obtained by measuring over 100 particles from the TEM image using Image J. A narrow distribution of the size can be observed with a mean diameter of 50 nm. The RSD was measured to be 10.62%, indicating that due to the independent optimization of the nucleation and the growth stage, uniform Ag nanoparticles have been obtained, which is highly appreciable for a wide range of SEF-based applications.

The preparation of the SANC was accomplished according to a previously reported method.[26] The conjugation of the GaH-IgG to the Ag nanoparticles can be confirmed from the TEM image in Fig. 2c. Compared with the bare Ag nanoparticles shown in Fig. 2a, a coating layer can be identified surrounding the dark core of the SANCs, in consistent with the previous reports. Extinction spectra were also measured for the Ag nanoparticles and the SANCs, as shown in Fig. 2d. A strong surface plasmon band with an extinction peak at 409 nm is exhibited in the spectrum of the Ag nanoparticles, as shown by the black line. It can also be observed that the full width at half maximum (FWHM) of the extinction spectrum is relatively narrow, which is attributed to the good homogeneity of the Ag nanoparticles. With the proteins attached to the Ag surface, the SANCs exhibit a red-shifted extinction peak at the wavelength of 421 nm. This is attributed to the increased local refractive index induced by the attached proteins.[36] Besides, the plasmon band is broadened, possibly due to the partial aggregation of the nanoparticles during the protein adsorption and the multiple purification processes. Consequently, the successful preparation of the SANCs has been confirmed by both the extinction spectroscopy and the TEM images.

Characterization of the fluorescence pre-quenched immune substrate

Glass-based fluorescence immune substrates can apply to a wide range of antibodies with simple procedures, avoiding the inconvenience in the uses of both the dye-labeled antibodies

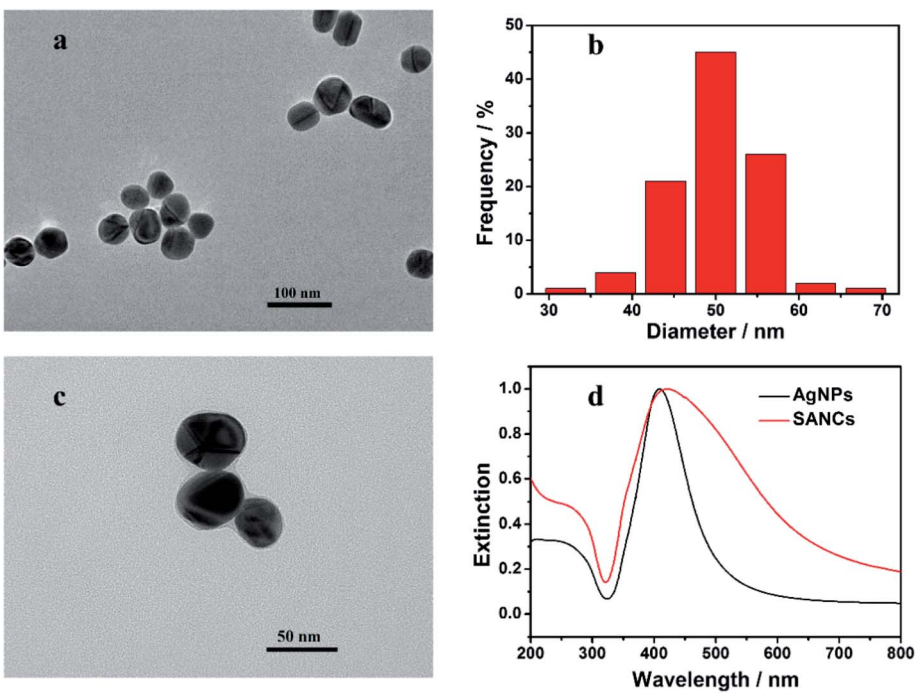

Fig. 2 The TEM image (a) and the size distribution histogram (b) of the Ag nanoparticles. (c) The TEM image of the SANCs. (d) The extinction spectra of the Ag nanoparticles and the SANCs.

and the metallic nanostructured substrates. However, the large blank signal limits the LOD that can be obtained. Silicon has been reported to quench the fluorescence of nearby emitters. Moreover, compared with the traditional quenching substrates such as Au or Ag thin films, the silicon substrates are more readily available and are hence used here for fluorescence pre-quenching. Due to the long-term exposure to the air, a thin oxide layer was formed on the silicon surface, so similar chemical manipulations can be performed on the silicon as those on the glass substrates. After the modification with PEI, an amine-rich polyelectrolyte, the RB molecules with carboxyl groups can be attached to the modified surface of the silicon substrate through the EDC/NHS crosslinking protocol. The concentration and the incubation time have been controlled so that only parts of the amino groups reacted with the RB molecules, while the rest of them reacted with GA to obtain the protein reactivity. For a valid comparison, RB molecules with the same surface density were attached to the silicon and the glass immune substrates, according to the method described in the Experimental section. The fluorescence spectra were recorded and shown in Fig. 3a. The fluorescence spectrum of the glass substrate is characterized by the black curve, which clearly indicates the presence of RB on the substrate. On the silicon substrate, a fluorescence signal with the same profile can also be observed, but with a significantly lower intensity, as shown by the red curve. Comparing the fluorescence intensity of the two substrates, an approximately 40-fold reduction of fluorescence can be observed on the silicon substrate. This corresponds to a quenching efficiency of around 97.5% compared with the glass substrate, thus validating the silicon-based pre-quenching effect. Ellipsometry measurements were performed to determine the distance between the RB molecules and the silicon surface. The thicknesses of the PEI layer with and without RB attachment (see the ESI, Fig. S1†) as well as the oxide layer were measured, and the result shows that the distance was controlled within a range of 3.36–3.94 nm. This distance range is consistent with the observed strong fluorescence quenching. It should be noted that besides RB, the quenching effect can also be observed for other fluorophores (see the ESI, Fig. S2†). This offers additional possibilities to tune the spectral range in the presented scheme to avoid the possible fluorescence interference from the impurities. The observed weak inherent fluorescence on the silicon substrate helps to maintain an ideal "OFF" state in the following immunoassay procedures.

Besides the low inherent fluorescence, the fluorescence enhancement effect is another factor that affects the assay performance. Metallic nanoparticles have been introduced as efficient fluorescence enhancers when dispersed onto fluorescent substrates, in the form of either bare or shell-isolated nanoparticles.[37–39] A similar procedure was employed to characterize the fluorescence enhancement effect of the immune substrates. Ag nanoparticles were drop cast in repeated cycles onto both the glass and the silicon immune substrates, and the fluorescence enhancement factors were recorded and compared, as shown in Fig. 3b. On the glass-based fluorescence immune substrate, the fluorescence was enhanced by the deposited Ag nanoparticles. It can be observed from the red line that the enhancement factor first increases and then tends to saturate with the increasing deposition cycles, which is in consistent with the previous reports.[39] The mechanism of the SEF effect has been investigated for decades. However, it is not an easy task to differentiate the different contributions for a specific situation. In the present case, the close proximity of the Ag nanoparticles enhances the excitation field at the location of the RB molecules. Moreover, the out-coupling of the energy transferred from RB to the Ag nanoparticles may also increase the emitted photons that can be detected. Consequently, each Ag nanoparticle exhibits an SEF effect on the nearby RB molecules on the substrate surface. At the early stage, the increased number of Ag nanoparticles leads to a larger fraction of RB molecules to be enhanced, resulting in the observed EF increase with the deposition cycles. As the deposition cycle number further increases, the closely stacked nanoparticles may make it difficult for the excitation light to fall onto the RB molecules and for the fluorescence to emit out through the nanoparticle layer. This effect is opposite to the SEF effect and may account for the observed saturation. A maximum enhancement factor of around 7.6 was observed. In comparison, the fluorescence enhancement factor of RB from the

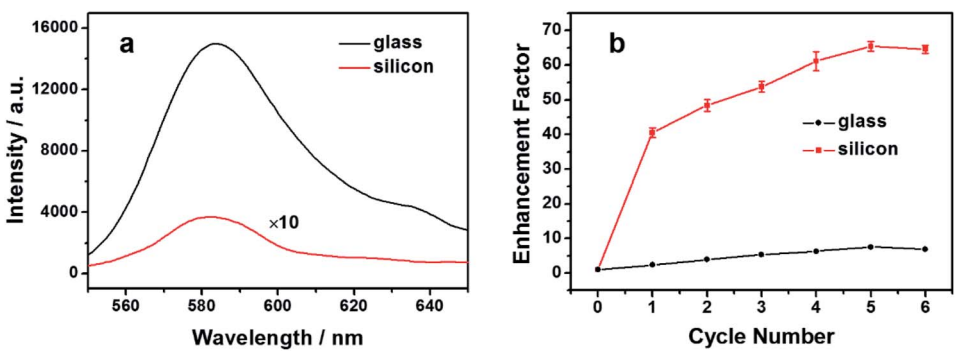

Fig. 3 (a) The fluorescence spectra measured from the fluorescence immune substrates based on glass (black) and silicon (red). The latter spectrum has been multiplied by 10 for clarity. (b) The dependence of the fluorescence EF on the number of Ag nanoparticle deposition cycles on the fluorescence immune substrates based on glass (black) and silicon (red).

silicon-based immune substrate exhibits a similar trend, as shown by the black line. However, the maximum value is significantly higher, reaching a factor of around 65.4. The pre-quenching effect of the silicon substrate is considered to play an important role in the observed higher EF. It has been reported that emitters with lower quantum yields are more apt to be enhanced compared with the ones with higher quantum yields.[40] The RB molecules are in close proximity to the silicon surface, which may provide additional non-radiative relaxation channels for the molecules, and hence the apparent quantum yield of the overall RB molecules is lowered.[29] A higher EF is consequently observed. Besides, the silicon substrate has also been reported to have an active effect on the SEF effect.[41] The optical near field may undergo a redistribution due to the presence of a nearby silicon substrate, which may also affect the fluorescence enhancement. More work is needed to determine the exact contribution of the silicon-assisted SEF effect. Importantly, both the low fluorescence background and the high EF obtained from the silicon substrate are highly appreciable for a sensitive "ON–OFF" immunoassay design.

Besides the appreciable optical properties, the fluorescence pre-quenched immune substrate is also protein reactive, as evidenced by the following immunoassay result shown in Fig. 4.

SEF-based immunoassay

The specificity of the presented immunoassay was evaluated prior to the LOD. As shown by the purple curve in Fig. 4, an inherent fluorescence can be observed form the immune substrate, which is relatively weak due to the silicon-based pre-quenching effect. Incubation with the SANCs was performed on the fluorescence pre-quenched immune substrates with either the HIgG or the BSA immobilization. In the case of 100 ng mL^{-1} of BSA immobilization, almost no change is observed in the fluorescence intensity as shown by the cyan curve, suggesting that the "OFF" state still remains. In the case of IgG with the same concentration, however, a significantly enhanced fluorescence is observed as shown by the red curve, which clearly indicate the "ON" state. The high contrast in the fluorescence intensity between the two cases is a clear indication of the good specificity of the presented immunoassay scheme.

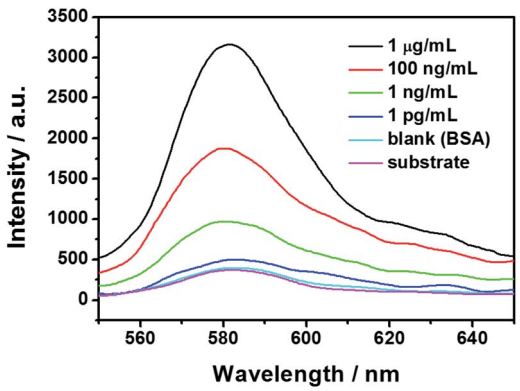

Fig. 4 The fluorescence spectra measured from the fluorescence pre-quenched immune substrates before (purple) and after the immune reaction with the SANCs at HIgG concentrations of 1 μg mL^{-1} (black), 100 ng mL^{-1} (red), 1 ng mL^{-1} (green) and 1 pg mL^{-1} (blue). The nonspecific fluorescence spectrum is also shown by the cyan curve.

The fluorescence spectra corresponding to the antigen concentrations ranging from 0.1 pg mL^{-1} to 1 μg mL^{-1} were measured and some typical spectra are shown in Fig. 4. It can be observed that the fluorescence intensity increases with increasing concentration of the target antigen in the current concentration range. In the case of 1 μg mL^{-1} of HIgG immobilization, an enhancement factor of up to 8.7 is observed, as shown by the black curve. Lower HIgG concentrations resulted in lower fluorescence enhancements, with only slightly enhanced fluorescence in the case of 1 pg mL^{-1}. The observed concentration-dependent fluorescence intensity can be accounted for by the varying surface density of the adsorbed SANCs through the immunoreaction. As the antigen concentration increases, more antigens were immobilized on the immune substrates, and consequently more SANCs were expected to be adsorbed onto the substrate surface through the antigen–antibody interaction. The increased surface density of the SANCs leads to the larger fluorescence enhancement. SEM images were also taken to show the surface morphology of the SANC-attached fluorescence pre-quenched substrates in the case of two different HIgG concentrations. In the case of 100 ng mL^{-1}, the SANCs are observed to distribute on the substrate surface with a relatively high surface density, as shown in Fig. 5a. In comparison, in the case of 1 pg mL^{-1}, only sparsely distributed SANCs are observed as shown in Fig. 5b, resulting in the much weaker fluorescence intensity. The fluorescence dependence on the nanoparticle surface density has been reported both on the glass substrates and on the metallic films. Here we have demonstrated that similar results can be observed on the silicon substrate, which is highly appreciable for practical applications due to the lower background and lower cost compared with the glass substrates and the metallic films, respectively.

The analytical performance of the presented immunoassay scheme was investigated and the results are shown by the red data points in Fig. 6a. Each data point and its error bar represent the mean and the standard deviation of three independently measured fluorescence intensities. The calibration curve was also depicted accordingly as shown by the red curve. The data were fitted well using an exponential logistic plot with a correlation coefficient (R^2) of 0.99668. This clearly demonstrates the analytical ability of the presented immunoassay scheme. It should be noted that among the various SEF-based immunoassays, only a few have demonstrated satisfactory analytical performances, possibly due to the heterogeneous nature of the generally used metallic nanostructured substrates.[17] In the presented scheme, the Ag nanoparticles are used as exogenous enhancers instead of the underlying substrate, thus eliminating the above-mentioned problem. The small standard deviations of the data points shown in Fig. 6a suggests that the presented scheme has a good repeatability. This renders the immunoassay a high analytical performance to determine the unknown antigen concentration with high accuracy. Besides, the LOD of the presented silicon-based

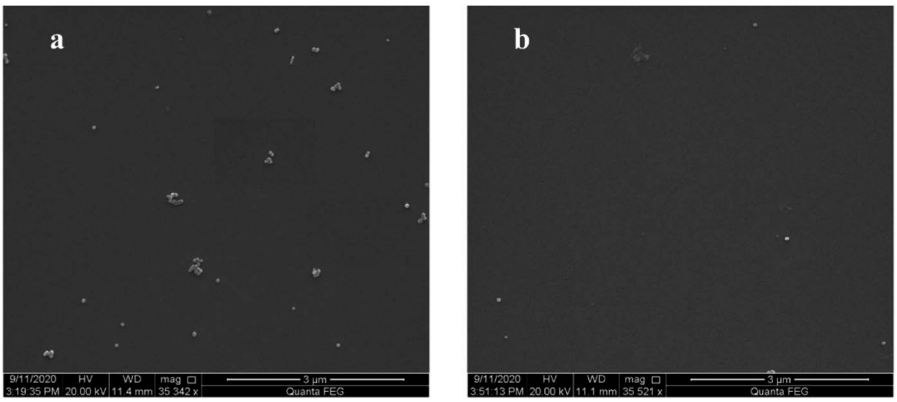

Fig. 5 The SEM images of the SANC-attached fluorescence pre-quenched immune substrate with different HIgG concentrations. (a) 100 ng mL^{-1}. (b) 1 pg mL^{-1}.

immunoassay scheme is determined to be 31.4 pg mL^{-1}, which is over an order of magnitude lower than that obtained from the glass-based scheme.[26] For a valid comparison, a similar immunoassay was also performed using glass substrates instead of the silicon substrates, and all the other conditions were kept identical. The results are shown by the black data points in Fig. 6a. It can be observed that the fluorescence intensities of the glass-based immunoassay are much higher than those of the silicon-based immunoassay. The standard deviations of the data points are also much larger in the glass-based immunoassay. A higher LOD of 0.631 ng mL^{-1} can be determined from the calibration curve of the glass-based immunoassay. The low LOD obtained in our presented scheme is extremely attractive for ultrasensitive immunoassays.

Suggested by the International Union of Pure and Applied Chemistry (IUPAC), the LOD is assigned from the calibration curve based on three standard deviations above the blank signal, corresponding to a confidence level of about 90%. Consequently, the reproducibility of the blank signal is a key factor of the LOD. Fluorescence measurements were performed on a total of ten batches of fluorescence pre-quenched immune substrates and the blank signals were shown by the red data points in Fig. 6b. For comparison, the fluorescence intensities of ten batches of glass immune substrates were also measured and shown by the black data points. It can be observed that the inherent fluorescence intensities from the silicon immune substrates are effectively suppressed due to the pre-quenching effect, exhibiting an ideal "OFF" state. Moreover, the corresponding standard deviations are also significantly smaller than that of the glass immune substrates, which is considered to contribute a lot to the observed low LOD. Besides, measurements from different batches of the immune substrates were also performed. Out of the ten batches of the silicon-based immune substrates, eight of them exhibit an inherent fluorescence intensity within a ±10% range of the average value, with an RSD of 7.07%. The observed low and highly reproducible blank signals between different batches make the presented scheme highly appreciable for practical applications.

The proposed immunoassay scheme offers several advantages over previously reported methods. Compared with conventional SEF-based methods, where fluorescently-labeled antibodies are needed to detect the specific target antigen,

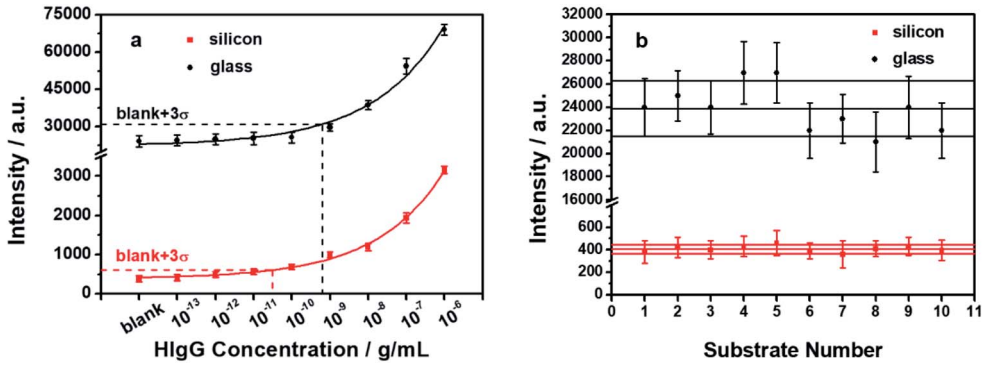

Fig. 6 (a) The calibration curves of the fluorescence signal *vs.* the concentration of HIgG obtained from the fluorescence pre-quenched immune substrates (red) and the glass immune substrates (black). The error bars represent standard deviations of three independent measurements of each concentration. (b) The inherent fluorescence intensities from ten batches of the silicon- (red) and glass-based (black) immune substrates. Each data point and its error bar represent the mean and the standard deviation of three independent measurements from each batch. The straight lines indicate 90%, 100% and 110% the intensity of the average from the ten batches, respectively.

unlabeled antibodies are used in our scheme. The complex chemistries during the labeling process are therefore avoided. The application range is hence broadened and the overall cost is reduced. Besides, in conventional SEF-based methods, the functionality of the labeled antibody may be affected. The antibody may be inactivated by labeling due to possible conjugation reactions at the active site, especially when multiple fluorophores are labeled on a single antibody.[25] In our scheme, without the need of labeling, the above effect has been circumvented. Although not directly evaluated, a good antibody functionality is suggested by the satisfactory immunoassay results in the presented scheme. Moreover, compared with the glass-based fluorescence immune substrate, the presented silicon substrate exhibits a significantly lower blank signal with higher reproducibility, which is responsible for the lower LOD.

Conclusions

In this paper, we have introduced a sensitive "ON–OFF" fluorescence immunoassay based on silicon-assisted SEF effect. A silicon-based fluorescence pre-quenched immune substrate has been constructed and used for antigen immobilization. The silicon substrate offers a very low blank signal due to the fluorescence quenching effect, which represents the "OFF" state. The SANCs have been synthesized for specifically recognizing the surface-immobilized antigens. The capture of the SANCs by the surface-immobilized antigen leads to an effectively enhanced fluorescence to produce an "ON" state. The analytical performance has also been investigated. Benefiting from the low and reproducible blank signal and the effective fluorescence enhancement, an LOD of 31.4 pg mL^{-1} is obtained. The presented scheme is straightforward, cost effective and sensitive, and is hence expected to find widespread applications in immunoassays as well as other fluorescence-based assays.

Conflicts of interest

There are no conflicts to declare.

Acknowledgements

This work was supported by the National Natural Science Foundation of China (NSFC) (No. 61601118) and Natural Science Foundation of Jiangsu Province (BK20140635).

References

1 G. Hawa, in Fluorescence in Industry, *Springer Series on Fluorescence (Methods and Applications)*, ed. B. Pedras, Springer, Cham, Switzerland, 2019, Application of Fluorescence in Life Sciences for Basic Research and Medical Diagnostics, vol. 18, pp. 341–364.
2 J. P. Gosling, A decade of development in immunoassay methodology, *Clin. Chem.*, 1990, **36**, 1408–1427.
3 E. Fort and S. Grésillon, Surface enhanced fluorescence, *J. Phys. D: Appl. Phys.*, 2008, **4**, 013001.
4 J. Dong, Z. Zhang, H. Zheng and M. Sun, Recent progress on plasmon-enhanced fluorescence, *Nanophotonics*, 2015, **4**, 472–490.
5 J. Li, C. Li and R. Aroca, Plasmon-enhanced fluorescence spectroscopy, *Chem. Soc. Rev.*, 2017, **46**, 3962–3979.
6 P. Anger, P. Bharadwaj and L. Novotny, Enhancement and quenching of single-molecule fluorescence, *Phys. Rev. lett.*, 2006, **96**, 113002.
7 S. Kühn, U. Håkanson, L. Rogobete and V. Sundoghdar, Enhancement of single-molecule fluorescence using a gold nanoparticle as an optical nanoantenna, *Phys. Rev. lett.*, 2006, **97**, 017402.
8 P. P. Pompa, L. Martiradonna, A. D. Torre, F. D. Sala, L. Manna, M. D. Vittorio, F. Calabi, R. Cingolani and R. Rinaodi, Metal-enhanced fluorescence of colloidal nanocrystals with nanoscale control, *Nat. Nanotechnol.*, 2006, **1**, 126–130.
9 J. R. Lakowicz, Y. Shen, S. D'Auria, J. Malicka, J. Fang, Z. Gryczynski and I. Gryczynski, Radiative decay engineering: 2. Effects of silver island films on fluorescence intensity, lifetimes, and resonance energy transfer, *Anal. Biochem.*, 2002, **301**, 261–277.
10 J. I. Gersten and A. Nitzan, Spectroscopic properties of molecules interacting with small dielectric particles, *J. Chem. Phys.*, 1981, **75**, 1139–1152.
11 R. Ruppin, Decay of an excited molecule near a small metal sphere, *J. Chem. Phys.*, 1982, **76**, 1681–1684.
12 J. R. Lakowicz, Radiative decay engineering 5: metal-enhanced fluorescence and plasmon emission, *Anal. Biochem.*, 2005, **337**, 171–194.
13 T. Ming, L. Zhao, H. Chen, K. C. Woo, J. Wang and H. Lin, Experimental evidence of plasmophores: plasmon-directed polarized emission from gold nanorod–fluorophore hybrid nanostructures, *Nano Lett.*, 2011, **11**, 2296–2303.
14 W. Deng, F. Xie, H. T. Baltar and E. M. Goldys, Metal-enhanced fluorescence in the life sciences: here, now and beyond, *Phys. Chem. Chem. Phys.*, 2013, **15**, 15695–15708.
15 Y. Jeong, Y. Kook, K. Lee and W. Koh, Metal Enhanced Fluorescence (MEF) for Biosensors: General Approaches and A Review of Recent Developments, *Biosens. Bioelectron.*, 2018, **111**, 102–116.
16 E. Matveeva, Z. Gryczynski, J. Malicka, I. Gryczynski and J. R. Lakowicz, Metal-enhanced fluorescence immunoassays using total internal reflection and silver island-coated surfaces, *Anal. Biochem.*, 2004, **334**, 303–311.
17 R. Nooney, A. Clifford, X. Leguevel, O. Stranik, C. Mcdonagh and B. D. Maccraith, Enhancing the analytical performance of immunoassays that employ metal-enhanced fluorescence, *Anal. Bioanal. Chem.*, 2010, **396**, 1127–1134.
18 R. Zhang, Z. Wang, C. Song, J. Yang, A. Sadaf and Y. Cui, Immunoassays based on surface-enhanced fluorescence using gap-plasmon-tunable Ag bilayer nanoparticle films, *J. Fluoresc.*, 2013, **23**, 71–77.
19 L. Zhou, F. Ding, H. Chen, W. Ding, W. Zhang and S. Y. Chou, Enhancement of immunoassay's fluorescence and detection sensitivity using three-dimensional

plasmonic nano-antenna-dots array, *Anal. Chem.*, 2012, **84**, 4489–4495.

20 B. D. Ventura, M. Gelzo, E. Battista, A. Alabastri, A. Schirato, G. Castaldo, G. Corso, F. Gentile and R. Velotta, Biosensor for point-of-care analysis of immunoglobulins in urine by metal enhanced fluorescence from gold nanoparticles, *ACS Appl. Mater. Inter.*, 2019, **11**, 3753–3762.

21 S. M. Tabakman, L. Lau, J. T. Robinson, J. V. Price, S. Sherlock, H. Wang, B. Zhang, Z. Chen, J. J. A. Tangsombatvisit, P. J. Utz and H. Dai, Plasmonic substrates for multiplexed protein microarrays with femtomolar sensitivity and broad dynamic range, *Nat. Commun.*, 2011, **2**, 466.

22 B. Zhang, R. B. Kumar, H. Dai and B. J. Feldman, A plasmonic chip for biomarker discovery and diagnosis of type 1 diabetes, *Nat. Med.*, 2014, **20**, 948–953.

23 B. Zhang, B. A. Pinsky, J. S. Ananta, S. Zhao, S. Arulkumar, H. Wan, M. K. Sahoo, J. Abeynayake, J. J. Waggoner, C. Hopes, M. Tang and H. Dai, Diagnosis of Zika virus infection on a nanotechnology platform, *Nat. Med.*, 2017, **23**, 548.

24 X. Li, T. Kuznetsova, N. Cauwenberghs, M. T. Wheeler, H. T. Maecker, J. C. Wu, F. Haddad and H. Dai, Autoantibody profiling on a plasmonic nano-gold chip for the early detection of hypertensive heart disease, *P. Natl. Acad. Sci. U. S. A*, 2017, **114**, 7089–7094.

25 S. Vira, E. Mekhedov, G. Humphrey and P. S. Blank, Fluorescent-labeled antibodies: Balancing functionality and degree of labeling, *Anal. Biochem.*, 2010, **402**, 146–150.

26 R. Zhang, Z. Wang, C. Song, J. Yang and Y. Cui, A straightforward immunoassay applicable to a wide range of antibodies based on surface enhanced fluorescence, *J. Fluoresc.*, 2013, **23**, 551–559.

27 C. Li, J. Gao, J. Yi, X. Zhang, X. Cao, M. Meng, C. Wang, Y. Huang, S. Zhang, D. Wu, C. Wu, J. Xu, Z. Tian and J. Li, Plasmon-enhanced ultrasensitive surface analysis using Ag nanoantenna, *Anal. Chem.*, 2018, **90**, 2018–2022.

28 D. Byrne and C. McDonagh, In situ generation of plasmonic cavities for high sensitivity fluorophore and biomolecule detection, *Nanoscale*, 2018, **10**, 18555–18564.

29 L. Danos, R. Greef and T. Markvart, Efficient fluorescence quenching near crystalline silicon from Langmuir–Blodgett dye films, *Thin Solid Films*, 2008, **516**, 7251–7255.

30 B. Yuan, X. Jiang, C. Yao, M. Bao, J. Liu, Y. Dou, Y. Xu, Y. He, K. Yang and Y. Ma, Plasmon-enhanced fluorescence imaging with silicon-based silver chips for protein and nucleic acid assay, *Anal. Chim. Acta*, 2017, **955**, 98–107.

31 H. Lu, L. Zhu, C. Zhang, Z. Wang, Y. Lv, K. Chen and Y. Cui, Highly uniform SERS-active microchannel on hydrophobic PDMS: a balance of high reproducibility and sensitivity for detection of proteins, *RSC Adv.*, 2017, **7**, 8771–8778.

32 C. Zhang, Z. Zhang, B. Yu, J. Shi and X. Zhang, Application of the biological conjugate between antibody and colloid Au nanoparticles as analyte to inductively coupled plasma mass spectrometry, *Anal. Chem.*, 2002, **74**, 96–99.

33 X. Chu, X. Fu, K. Chen, G. Shen and R. Yu, An electrochemical stripping metalloimmunoassay based on silver-enhanced gold nanoparticle label, *Biosens. Bioelectron.*, 2005, **2**, 1805–1812.

34 J. Ling, Y. F. Li and C. Z. Huang, Visual sandwich immunoassay system on the basis of plasmon resonance scattering signals of silver nanoparticles, *Anal. Chem.*, 2009, **81**, 1707–1714.

35 P. C. Lee and D. Meisel, Adsorption and surface-enhanced Raman of dyes on silver and gold sols, *J. Phys. Chem.*, 1982, **86**, 3391–3395.

36 J. J. Mock, D. R. Smith and S. Schultz, Local refractive index dependence of plasmon resonance spectra from individual nanoparticles, *Nano lett*, 2003, **3**, 485–491.

37 S. Pan, Z. Wang and L. J. Rothberg, Enhancement of adsorbed dye monolayer fluorescence by a silver nanoparticle overlayer, *J. Phys. Chem. B*, 2006, **110**, 17383–17387.

38 A. R. Guerrero and R. F. Aroca, Surface-enhanced fluorescence with shell-isolated nanoparticles (SHINEF), *Angew. Chem., Int. Ed.*, 2011, **50**, 665–668.

39 R. Zhang, Z. Wang, C. Song, J. Yang, J. Li, A. Sadaf and Y. Cui, Surface-Enhanced Fluorescence from Fluorophore-Assembled Monolayers by Using Ag@SiO_2 Nanoparticles, *ChemPhysChem*, 2011, **12**, 992–998.

40 K. Munechika, Y. Chen, A. F. Tillack, A. P. Kulkarni, I. J. Plante, A. M. Munro and D. S. Ginger, Spectral control of plasmonic emission enhancement from quantum dots near single silver nanoprisms, *Nano lett*, 2010, **10**, 2598–2603.

41 S. Guo, S. Tsai, H. Kan, D. Tsai, M. R. Zachariah and R. J. Phaneuf, The Effect of an Active Substrate on Nanoparticle-Enhanced Fluorescence, *Adv. Mater.*, 2008, **20**, 1424–1428.